SKIN FRICTION AND TRANSITION LOCATION MEASUREMENTS ON SUPERSONIC TRANSPORT MODELS

ROBERT A. KENNELLY JR.[1] and AGA M. GOODSELL[1]

Keywords: skin friction, oil-film, interferometry, transition, sublimation, supersonic

ABSTRACT

Flow visualization techniques were used to obtain both qualitative and quantitative skin friction and transition location data in wind tunnel tests performed on two supersonic transport models at Mach 2.40. Oil-film interferometry was useful for verifying boundary layer transition, but careful monitoring of model surface temperatures and systematic examination of the effects of tunnel start-up and shutdown transients will be required to achieve high levels of accuracy for skin friction measurements. A more common technique, use of a subliming solid to reveal transition location, was employed to correct drag measurements to a standard condition of all-turbulent flow on the wing. These corrected data were then analyzed to determine the additional correction required to account for the effect of the boundary layer trip devices.

1 INTRODUCTION

The goal of NASA's recently concluded High Speed Research (HSR) Program was to develop technologies in support of a 300 passenger, 5000 nautical mile, Mach 2.4 aircraft [1]. To reduce the risk in this ambitious undertaking, new levels of precision and accuracy in wind tunnel testing were required. Improved flow visualization has played a role. Two of the flow visualization techniques applied in supersonic cruise performance testing for the HSR Program will be presented. The first, oil-film interferometry, is a relatively new method for skin friction measurement; it may also be used to determine boundary layer state. Transition indication using a subliming chemical solid is a well-known technique, but its quantitative application to laminar run and trip drag corrections is less common. These flow visualization efforts were directed toward developing post-test data corrections that permitted drag data to be reported for fully turbulent flow on the model, while accounting for the drag of the boundary layer trip devices.

Modern CFD methods are good enough that computed drag levels are frequently accurate to within a few percent for attached flow on simple configurations. Aside from a secondary role as insurance against gross computational blunders, cruise performance wind tunnel testing is pointless unless it can achieve equal or better accuracy. This requires that all aspects of testing, from model fabrication to final data corrections, be carried out with high precision.

1.1 Experimental Facility

The flow visualization results to be presented were obtained in the NASA Langley Research Center (Hampton, VA, USA) Unitary Plan Wind Tunnel [2]. This is a closed circuit, pressurized, continuous flow, supersonic facility capable of Mach numbers from 1.47 to 4.63. The present work was performed in Test Section #2 at Ma = 2.40 and Reynolds numbers of 3.0 and 4.0 million/ft (9.85 and 13.13 million/m). The test section is 4-ft (1.22 m) square by 7-ft (2.13 m) long; this

Author(s): [1] *NASA Ames Research Center, Moffett Field, CA 94035-1000, USA.*

Corresponding author: Robert A. Kennelly Jr., email RAKennelly@mail.arc.nasa.gov

modest size has negative implications for the post-run photography required by oil-film interferometry, but otherwise the optical access is good.

1.2 Wind Tunnel Models

The two test articles were 0.01675-scale supersonic transport models. The first, designated 'Ref H,' is a proprietary configuration. It was a control-effects model with segmented leading and trailing edges. The wing planform was a modified delta with two breaks. The second was a performance model of the Technology Concept Airplane (TCA) without pressure instrumentation or control surfaces. It, too, had a modified delta planform but only a single leading edge break. Both wings had subsonic, blunt leading edges inboard and sharp, supersonic leading edges outboard.

1.3 Overview

The paper consists of two principal parts: Section 3, concerned with oil-film interferometry, and Section 4, devoted to the sublimation study. Each part begins with a brief review of a method, followed by a detailed description of that technique as used in this work. Samples of the flow visualization results are presented, accompanied by quantitative measurements based on the images. Error estimates for these measurements are also discussed. We conclude in Section 5 with discussion of some issues uniting the two flow visualization approaches.

2 NOMENCLATURE

2.1 Symbols

$\Delta C_{D_{lam}}$	Drag correction for partially laminar boundary layer (add to measured drag)
$\Delta C_{D_{trip}}$	Correction for drag caused by boundary layer trip devices (subtract from measurement)
C_f	Skin friction coefficient, referenced to freestream conditions
f	Focal length
k	Trip disk height, also thermal conductivity
Ma	Mach number, V/a
n	Index of refraction
Pr	Prandtl number, $\mu c_p/k$
q	Dynamic pressure, $\rho V^2/2$
R	Coefficient of expansion of silicone oil, [K^{-1}]
Re	Reynolds number, $\rho VL/\mu$
S	Exponential rate of decrease of silicone oil kinematic viscosity, [K^{-1}]
t	Time
T	Temperature
V	Velocity
x	Streamwise distance

2.2 Greek Symbols

α	Angle of attack (deg)
λ	Wavelength of illumination
μ	Viscosity
ν	Kinematic viscosity, μ/ρ
ρ	Density
$\Delta\xi$	Interference fringe spacing

2.3 Subscripts

oil	Silicone oil (here, DC-200 Fluid)
ref	Calibrated reference condition for silicone oil properties (here, 40 °C)

wall	Conditions on surface of model
WT	Wind tunnel
0	Stagnation conditions
∞	Freestream reference conditions

2.4 Abbreviations and Acronyms

CFD	Computational fluid dynamics
EI	Exposure index
FWHM	Full-width at half-maximum
IR	Infrared
NASA	National Aeronautics and Space Administration (USA)
Ref H	Proprietary supersonic transport configuration
RMS	Root mean square
TCA	Technology Concept Airplane
UPWT	Unitary Plan Wind Tunnel
UV	Ultraviolet

3 SKIN FRICTION MEASUREMENT BY OIL-FILM INTERFEROMETRY

3.1 Background

Oil-film interferometry, originally known as the viscosity balance method, is a technique for direct measurement of skin friction. The shearing force exerted by a fluid flowing past a surface causes oil placed on the surface to thin with time. Using lubrication theory, the development of the oil film thickness profile can be related to the shearing force. According to the method as first proposed by Tanner et al. in the 1970s [3, 4], the transparent oil is applied in a line or as a group of dots to a piece of polished glass. The changing film thickness is measured over time by optical interferometry using a He-Ne laser. One of the interfering beams is the reflection from the front surface of the oil, while the other arises by reflection from the back surface of the glass. Since it is the variation of the combined optical thicknesses of the oil and the glass substrate that is being measured, the glass must be measured separately in order to deduce the thickness of the oil film. The requirement for a highly coherent light source and the restriction to transparent test surfaces make the original form of the oil-film technique impractical for most wind tunnel testing.

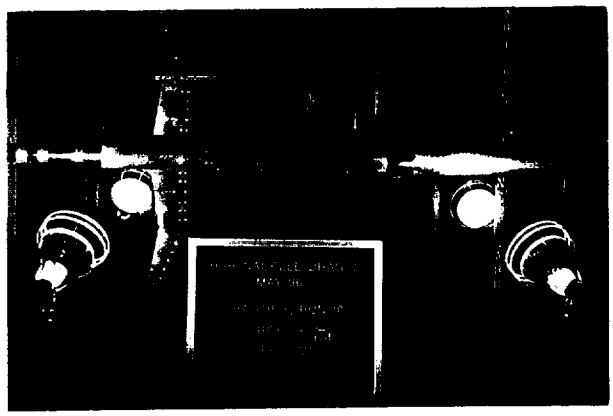

Figure 1. Ref H model prepared for oil-film interferometry run in Langley UPWT.

A low-cost alternative to using a polished glass substrate and a laser was developed by Monson and Mateer at NASA Ames Research Center [5, 6]. An optically smooth plastic film replaces the glass in Tanner's method. This is illustrated in Fig. 1, where the black patches on the

model consist of paint-and-adhesive-backed Mylar film, about 0.002 inch (0.05 mm) thick, sold for use by hobbyists as a model airplane covering (MonoKote, Top Flite Models, Champaign, IL, USA). Visible interference fringes are formed in the specular reflection of a broad, diffuse light source from the air-oil and oil-Mylar interfaces. In the low-cost form of the method, the illumination need not be highly coherent because the optical paths of the interfering beams are nearly identical. Thus no laser is required, a welcome simplification. Fringe contrast is good because the index of refraction of Mylar is 1.67, appreciably higher than that of the oil, which is approximately 1.40. By Fresnel's Law, the reflectivity of the two interfaces is 2.8% (for air-oil) and 0.75% (oil-Mylar) at normal incidence; these are evidently close enough for good fringe visibility. Tanner and Blows reported very weak reflection from the oil-glass interface and were therefore unable to obtain interference fringes representing only the thickness variation of the oil film. If their substrate was common crown glass with $n \approx 1.52$, the reflectivity would have been only 0.16%, one-fifth that of the oil-Mylar interface. Usable fringes can also be obtained with oil placed directly on polished stainless steel surfaces (approx. 2 micro-inch RMS roughness), but image contrast is not as good as with oil-on-Mylar, and it is difficult to maintain such high surface quality.

Oil-film interferometry in its simplified form has been demonstrated in a variety of settings in recent years. It was used in a production wind tunnel test in 1994, as presented by Kennelly et al. at the 7th ISFV [7]. Other wind tunnel applications are described by Driver [8]. A detailed, low-speed study of the flow around boundary-layer trip disks was conducted by Drake [9]; selected aspects of that work were the subjects of a paper at the 8th ISFV [10] and a flow visualization poster [11]. Zilliac [12, 13] measured the skin friction associated with flow about a model wingtip. The oil-film technique has also been used in flight by Drake and Kennelly [14, 15]. The present investigation begins to extend the method into flow regimes where model heating has significant effects.

3.2 Technique

To determine surface shear, Tanner and Blows used fringe measurements from a series of interferograms to determine the time rate of change of the oil film slope. It would be difficult to obtain such a sequence of images in a large, pressurized wind tunnel where the flow must be stopped for photographic access. Subject to certain assumptions, the oil-film technique as applied here requires only a single fringe image, obtained following the run [3, 6, 8]. It is a direct method—no calibration is required. The result of the measurement is the component of local skin friction normal to the axis of the applied line of oil. The key assumptions are:

1. Oil thickness and flow velocity do not affect the airflow
2. Oil film is thin compared with its length, and its surface slope is small
3. Two-dimensional flow
4. Skin friction coefficient (not shear force) is constant during entire run
5. Initial oil thickness is large compared with final thickness
6. Shear is constant over the fringe measurement area

If these hold, the airflow causes the oil to thin into a wedge shape whose slope is inversely proportional to run time. The effects of gravity, pressure gradients, and surface tension are generally found negligible compared to the thinning due to shear. In the present work, the wing surface was almost horizontal and nearly flat, and there were no embedded shocks or separations. The most questionable assumption is probably that C_f is constant; we will return to this issue later. The analysis assumes steady flow, reasonable for the laminar boundary layers to which it was originally applied. So far unexamined is the implicit assumption that the response of the oil film to a turbulent boundary layer correctly reflects the time-averaged skin friction.

Mateer et al. [6] propose Eq. (1) for the reduction of oil-film fringe measurement data. It expresses the skin friction coefficient as a function of oil properties, integrated flow history, and end-of-run fringe spacing. The integral is the same for all measurement locations on the model with the same flow and surface temperature history; therefore, the skin friction is simply proportional to fringe spacing, $\Delta\xi$. In the simplified treatment to follow, only two values of the multiplicative factor, corresponding to laminar and turbulent surface temperatures, are required.

$$C_{f,\infty} = \frac{2(n\rho\nu)_{ref}}{\lambda \int_0^{t_{run}} q_\infty(t)\; e^{\left\{(S+R)\left[T(t)-T_{ref}\right]\right\}}\, dt} \cdot \Delta\xi \qquad (1)$$

Note that this skin friction coefficient is normalized to freestream conditions rather than to the flow at the edge of the boundary layer. Zilliac [12] presents alternatives to the simple exponential laws for oil density and kinematic viscosity embodied in the integral of Eq. (1). These laws may be preferable, especially in low-temperature applications, but the original form is adequate for the temperature range of the present work.

The oil film consists of DC-200 Fluid (Dow-Corning, Midland, MI, USA), a silicone polymer (polydimethylsiloxane) with typical composition $(CH_3)_3SiO[SiO(CH_3)_2]_nSi(CH_3)_3$. It is clear, non-toxic, and has a low vapor pressure. This work used oil whose nominal kinematic viscosity was 10,000 centistokes (cS), chosen to yield a convenient run time (see Section 3.3). Physical properties of DC-200 Fluid are summarized in Table 1. Refractive index, n, was obtained from the manufacturer for the 10,000 cS oil, while ρ_{ref} and R are simply typical of this family of silicone oils. The lapse rate of kinematic viscosity with temperature, S, was determined by calibration at 25, 35, and 45 °C (Gascoyne Labs., Baltimore, MD, USA). The viscosity decreases by about 1.7% per degree Celsius; this sensitivity is a significant source of uncertainty. We note that $S \gg R$, so at least the primary source of temperature variation has been checked, but n, ρ_{ref}, and R remain unevaluated sources of error. The quoted shelf life of DC-200 Fluid is one year, and there is evidence that the oil properties do change over time—it is probably worthwhile to evaluate all the relevant oil parameters shortly before or after each use. Our sample of 10,000 cS oil actually measured 8,803 cS (at 25 °C) two years after manufacture, while the oil viscosity reported by Dow-Corning was 10,034 cS. (The manufacturer's limits are 9,500 to 10,500 cS for fresh fluid.)

Table 1. Silicone oil properties (DC-200 Fluid, 10,000 cS nominal viscosity).

Oil Property	Value (T_{ref} = 40 °C)	Source	Uncertainty (estimated)
n	1.4036	nominal, per manufacturer	±0.001
ρ_{ref}	958 kg/m3	typical for DC-200 Fluids	±5
R	0.00096 K^{-1}	typical for DC-200 Fluids	–
ν_{ref}	6752 cS	calibrated	±50
S	0.01763 K^{-1}	calibrated	±0.00050

The illumination was effectively monochromatic. The lamps were 160 W high-intensity discharge, self-ballasted mercury reflector lamps with a strong green spectral peak at a wavelength of 546.1 nm (Iwasaki Electric Co., Tokyo, Japan). This peak was (fairly well) isolated by photographing through a green dichroic process filter centered on $\lambda \approx 540$ nm and with a pass-band width of 75 nm (FWHM). The average wavelength was found by calibration of the lamp/filter combination to be 555 nm, and this value was used for the data reduction. This average also takes into account the sensitivity of the film, which drops rapidly above 680 nm, and the UV filtration provided by the camera lens (Leica Camera AG, Solms, Germany), which blocks wavelengths shorter than 375 nm. We have since obtained a custom-designed interference filter (Andover Corp., Salem, NH, USA) that better isolates the strong peak at 546.1 nm. It has a width of less than 20 nm; this will eliminate any significant error due to wavelength uncertainty. The required broad, diffuse source was created by bouncing light from the lamps off a large white card. We have, on other occasions, also used light boxes with translucent white glass fronts containing fluorescent or mercury HID lamps; the latter require cooling ventilation.

A conventional 35-mm single-lens reflex camera, equipped with a 90-mm f/2.8 lens and supplementary close-up lens, was used to record the oil-film interference fringe patterns. Two different black-and-white films were used: T-Max 400 (ISO 400/27°) and Technical Pan, the latter

a copy film which can be specially developed for continuous tone reproduction (Eastman Kodak, Rochester, NY, USA). Exposure was determined using the camera's built-in light meter through the supplementary lens and green filter. A typical reading of the specular (glare) image of the illuminated card reflected in the black-paint-backed Mylar (against which the fringes are visible) was *f*/8 at 1 sec for Tech Pan rated at EI 100/21°. All exposures were bracketed by ±1 *f*-stop; this was critical for Tech Pan, which has very little exposure latitude. Object distance was about 18 inch (45 cm), so there was also very little depth of field. (Since the camera was tripod-mounted anyway, it might have been better to stop down and accept somewhat longer exposure times.) The two visualization examples shown below in Section 3.4 used Tech Pan film. Photographic prints of these images are grainless and very sharp, but the good results may not be worth the extra trouble required—prints from T-Max 400 negatives were also fully usable, and the higher film speed, less-critical exposure, and standard development process would all be helpful.

Fringe measurements on the model were located spatially in relation to model features such as joints and planform breaks. A machinist's scale was included in each photograph to provide a length reference. An image area with a typical dimension of 6 inch (15 cm) was large enough to include these features and to allow for fringe measurements at 20–30 locations. The dark bands were on the order of 2–5 mm apart, and in most cases this was derived from measuring two fringe spacings. Higher accuracy could be attained by imaging a smaller area, but this would make it more difficult to know where the measured points are located on the wing. A background grid of reference marks might help here, and would provide a means to assess whether the viewing angle is perpendicular to the wing surface. The photographic process, involving lamps, white card, camera, and tripod, was made more difficult by the small size of the wind tunnel. Although not the usual model orientation in the UPWT, it was easier to photograph the interference patterns with the model rolled 90 deg so that the imaged surface of the wing faced the open access door.

3.3 Oil-Film Experiment

The work to be described was performed over the course of three days in May 1996, as part of another test. Test conditions in the wind tunnel were as follows: Ma = 2.40, Re = 3.0 million/ft (9.85 million/m), T_0 = 125 °F (324.9 K). The optically smooth plastic surface was cleaned with alcohol (not detergent!) before each run. Three spanwise lines of silicone oil were applied, using the edge of a rubber squeegee, to patches of MonoKote located just inboard and outboard of the planform break (see Fig. 1).

Run duration was a compromise between testing cost and data quality. Longer runs ensure that the thinning of the oil film predominantly reflects the chosen flow conditions; a more complete study would quantify this by varying run time to establish that the effects of the tunnel transients are negligible. For this experiment, the run time consisted of 30 minutes 'on condition,' with 5–10 minutes required to start and stop the wind tunnel. DC-200 Fluid is available in a number of viscosities; one of these, 10,000 cS, was chosen to yield easily measured fringe spacings in this length of time.

Stagnation temperature, stagnation pressure, and test section static pressure were recorded at 30-sec intervals. The latter quantity permits calculation of the Mach number in the test section during the start-up and shutdown transients. Once supersonic flow is established in the test section, the Mach number is known from the calibrated nozzle setting. The flow conditions in the test section can then be used to compute $q(t)$ and $T_{oil}(t)$, required by the integral in Eq. (1) relating skin friction coefficient to fringe spacing. The only significant variation in the airflow occurs during the transients; once on condition, pressure and temperature are held constant to within ±0.1%.

3.4 Results

The brief test successfully demonstrated several aspects of oil-film interferometry as a *qualitative* visualization method. A number of interference fringes were clearly visible behind each oil line, see Figs. 2 and 3; the freestream flow direction is from right to left in both figures. Low contrast, widely spaced fringes created by interference within the Mylar itself can also be seen, but they did not interfere with the measurements. (An absorbing plastic film would eliminate these weak fringes

altogether.) Supersonic test conditions created a new problem: there were isolated spots where the Mylar film de-bonded from the underlying black paint layer (in Fig. 2, see the lighter-gray areas near the leading edge). In addition, a portion of the leading edge of one Mylar patch, visible in the upper third of Fig. 3, peeled up during one run. These defects may have been caused by the approximately 90 °F (32 °C) model surface temperature, exacerbated by using the same patches for two successive runs.

The first dark fringe (destructive interference) of each group appears downstream of the edge of the applied line of oil. This is because there is a 180 degree phase change in the reflected light at *both* the air-oil and oil-Mylar interfaces ($n_{air} < n_{oil} < n_{Mylar}$), and therefore the interference is constructive for the vanishing film thickness at the leading edge of the oil. What appear to be kinks in the middle and downstream oil lines of Figs. 2 and 3 are actually just the result of a sudden change in fringe spacing where a laminar region abuts an area with turbulent flow. Both the laminar and turbulent fringes actually originate from the same, unkinked line of oil, but because of constructive interference, its leading edge is not visible.

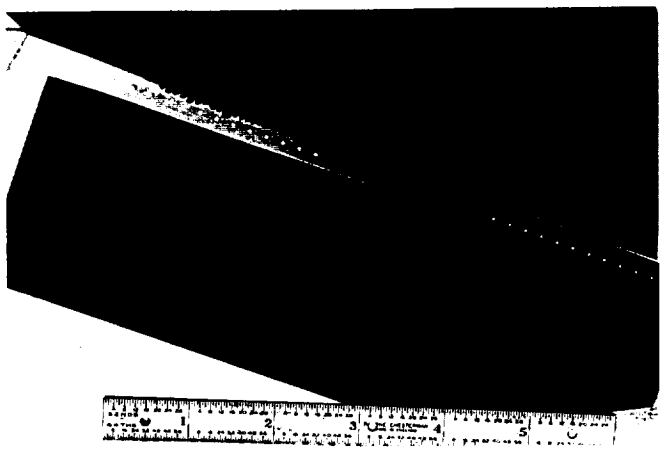

Figure 2. Oil-film interferogram, inboard of planform break (airflow is from right to left).

In both figures, the trip disks adjacent to the black hash marks on the leading edge are $k = 0.0095$ inch (0.24 mm) high, while the disks in the other set are $k = 0.015$ inch (0.38 mm) high. The disks are molded of automotive epoxy body filler compound using perforated tape; the disk spacing is 0.20 inch (5.08 mm) center-to-center. Between these two sets of disks is a bare region with no trip devices applied. Note that along each line of oil, the fringe spacing (and thus C_f) decreases with increasing distance from the leading edge, as would be expected for larger values of streamwise Reynolds number, Re_x. In both figures, the boundary layer remains laminar (closely spaced fringes) behind the free-transition portion of the leading edge as far as the last oil line. Along the sides of the laminar region, there is a distinct jump in fringe spacing where the region is bounded by turbulent flow stimulated by the trip disks.

It was not possible to learn very much from the ragged fringe pattern immediately behind the trip disks. Pronounced 'zigzags,' the result of flow features (horseshoe vortices and, perhaps, other structures [16, 17, 18]) created by the disks, made it difficult to draw any conclusions about the state of the boundary layer or the precise location of transition. An attempt to evaluate trip disk effectiveness by placing a line of oil a short distance behind and parallel to the disks was abandoned after a single trial. The zigzags in the interference fringes, which indicate variations in C_f, diminish gradually with streamwise distance (see esp. Fig. 2). These disk-induced disturbances have been studied in detail by Drake [9], who concluded that they do not cause a significant shift in the turbulent skin friction level downstream of the trip disks.

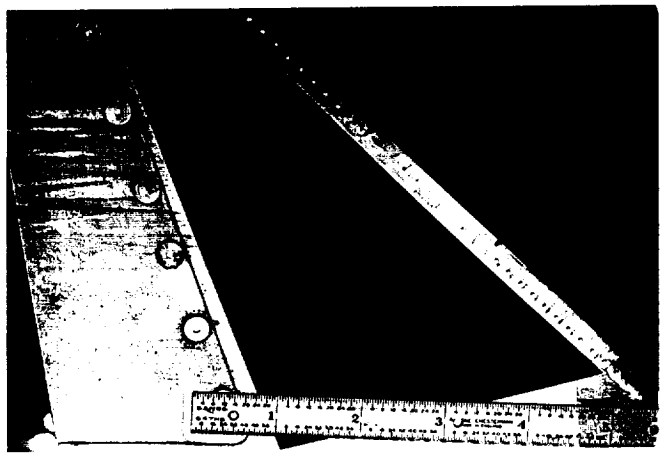

Figure 3. Oil-film interferogram, outboard; note damaged Mylar. Airflow is from right to left.

The same two images of the upper surface of the wing were analyzed to derive *quantitative* skin friction values. An example of the results obtained is presented in Fig. 4. These data are taken from the middle oil line in Fig. 3 and include both laminar (free transition) and turbulent (tripped) values downstream of the bare leading edge and the k = 0.015 inch (0.38 mm) disks, respectively. (No measurements were made behind the damaged MonoKote.) In the absence of surface temperature measurements, laminar and turbulent flat-plate recovery factors ($Pr^{1/2}$ and $Pr^{1/3}$, with Pr = 0.71) were used to estimate adiabatic wall temperature as a function of time (see, for example, the text by White [19], sect. 7-8.3). The oil temperature was assumed to be unaffected by the thermal conductivity and heat capacity of the model and thus to simply track the adiabatic wall temperature. The streamwise component (perpendicular to the applied line of oil) of the local skin friction, $C_{f,x}$, is plotted against span station expressed in full-scale aircraft inches. The error bars in the figure will be discussed in Section 3.5. Each data point arises from a fringe spacing measurement along the line of oil; note that the most outboard measurements are the ones closest to the leading edge of the wing. The turbulent data are more scattered for locations nearer to the trip disks, reflecting the zigzags in the fringes mentioned previously.

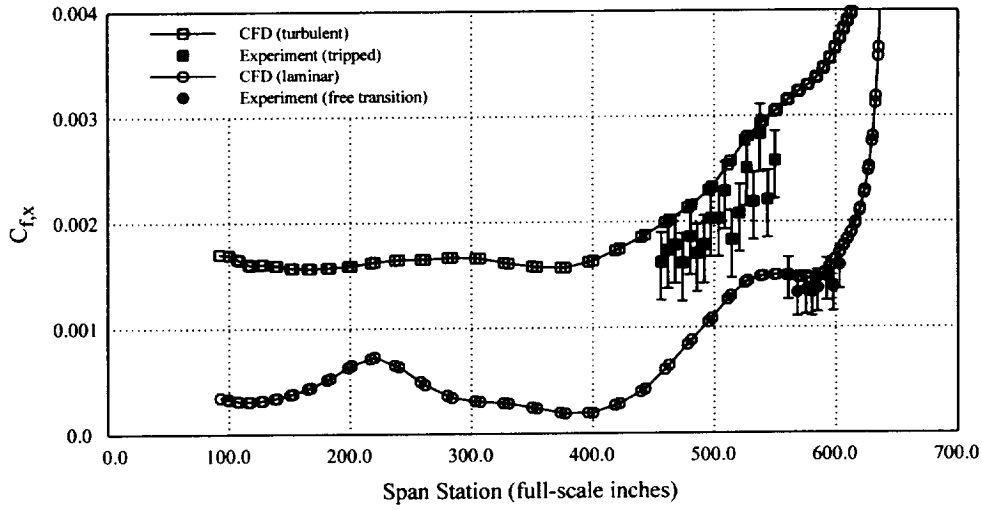

Figure 4. Measured and computed streamwise skin friction along a single spanwise oil line.

Also included in Fig. 4 are results of two Navier-Stokes calculations of the flow about the Ref H configuration at conditions matching the wind tunnel (Scott Lawrence, NASA Ames, private communication). One computation was fully laminar, while the other assumed fully turbulent flow using the Baldwin-Lomax turbulence model. The turbulent skin friction measurements, but not the laminar results, are seen to lie significantly below the CFD values. Since most other aspects of the measurements are the same for laminar and turbulent boundary layers, this suggests a possible temperature-dependent systematic error. The skin friction values derived from fringe spacing are temperature sensitive through the viscosity of the silicone oil. We can use the Navier-Stokes wall temperatures, shown in Fig. 5, to estimate the error resulting from our assumption of a flat-plate adiabatic wall. The turbulent flat-plate recovery temperature is 306.1 K, about 5 K above the calculations in the region of the wing where the turbulent fringes were measured. The corresponding laminar value is 297.5 K, which is roughly 3 K *below* the computed values. If the CFD temperatures are used in the experimental data reduction instead of the simple recovery factor estimates, the turbulent skin friction would increase by 10%, but the laminar values would *decrease* by 5%. Now both laminar and turbulent measurements are somewhat lower than the calculations—there may be a systematic error, but it no longer appears to be due solely to the estimated turbulent wall temperatures.

For a turbulent boundary layer, the data quoted by White [19, p. 555] and the present calculations both suggest that $r_{turb} = 0.88$ might be a better choice than $r_{turb} = Pr^{1/3} = 0.892$ if a recovery factor estimate must be used for T_{wall}. This would reduce the estimated wall temperature by about 2 K and bring it in line with the computed values. The better approach, given that the effects of pressure gradient, thermal conduction in the model, flow separation, etc., are unknown, would be to *measure* the surface temperature. Ideally, several measurements would be made during the run of the entire surface, perhaps using temperature-sensitive paint or IR thermography. But even a few spot measurements at locations of interest, perhaps augmented by computations to assist interpolation, would be an improvement. The assumption of flat-plate recovery temperatures is adequate for experimental planning, but it seems clear that actual measurements of surface temperature will be required for accurate skin friction measurements at supersonic Mach numbers.

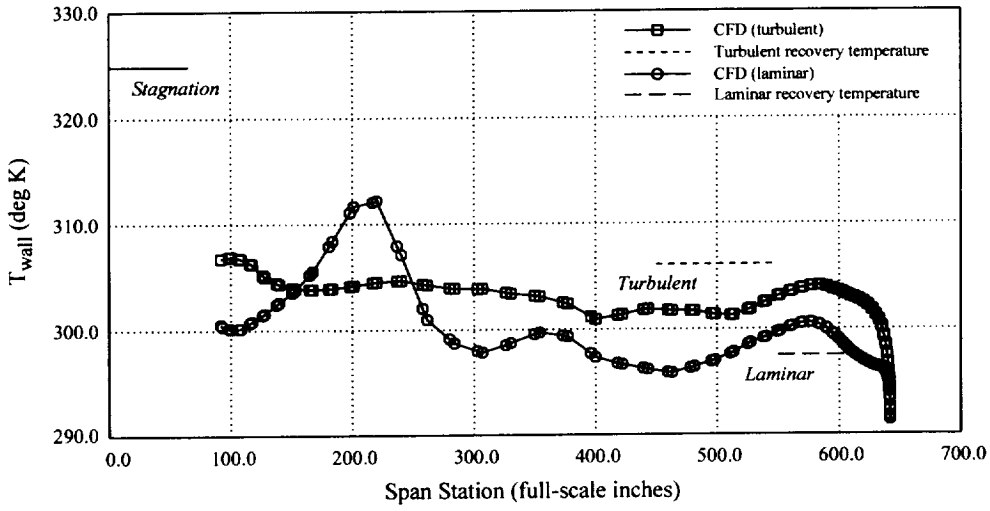

Figure 5. Computed and estimated upper surface wing surface temperatures.

Note that while some variation would be expected, the skin friction and temperature peaks in the 'CFD (laminar)' curves near Span Station 220 are probably not typical of attached flow. Indeed, examination of a more complete set of upper surface spanwise skin friction distributions reveals a similar peak-and-valley pattern that begins some distance upstream. This suggests the presence of a separation vortex in the fully laminar solution, the computational analogue of the type

of vortex/boundary layer interaction whose skin-friction footprint was studied by Westphal et al., to be presented at the 9th ISFV [18]. The peak in the computed T_{wall} distribution apparently arises from a distortion of the boundary layer temperature distribution caused by the vortex.

3.5 Errors

Experimental errors for the oil-film technique as applied here to supersonic testing are estimated to highlight what are believed to be the major areas for potential improvement. The skin friction data presented above in Fig. 4 included error bars based on the discussion to follow. Systematic issues related to the technique itself, analyzed in the references, are not included; the error limits plotted in the figure are thus somewhat optimistic.

In the absence of oil temperature measurements, the skin friction uncertainty from this source will be evaluated for $T_{oil} = T_{wall}$ *(est.)* ±5 K, an interval consistent with the difference between the flat-plate estimates and the computed temperatures (Fig. 5). This factor alone contributes almost 10% to the experimental uncertainty estimate; the actual values are given in Table 2.

Table 2. Estimated contributions to skin friction uncertainty.

	Laminar		Turbulent	
Oil temperature	+8.7%	–9.6%	+8.6%	–9.8%
Wind tunnel transients	+7.5%	–12.2%	+7.5%	–12.2%
Illumination wavelength	±3.6%			
Fringe spacing	±4%		±2%	
Oil properties	±1%			
Total (RMS)	+12.7%	–16.5%	+12.2%	–16.2%

Again lacking a measurement of the effect, a plausible estimate is offered for the uncertainty due to the assumption that the skin friction *coefficient* is constant during the wind tunnel start-up and shutdown. The frictional forces acting on the oil film during the transients are assumed to be half or double those assumed implicitly for constant $C_{f,x}$; note that the effect on the measured quantity is asymmetrical. This approach has yielded error estimates consistent with observations for a set of runs of varied length obtained during another experiment (Russell Westphal, Washington State University, private communication).

The accuracy of the illumination wavelength is estimated to be ±20 nm relative to the 555 nm weighted average of the light from the combined Hg lamp and green filter. This estimate is based on the separation between the average wavelength and the nearby spectral peaks at 577.0 and 579.1 nm, which are not fully extinguished by the filter. Uncertainty in λ contributes almost ±4% to the skin friction error, a figure that could be improved to <1% through use of an interference-type notch filter centered on 546.1 nm, the largest spectral peak of the lamp.

Fringe spacings were measured from photographic enlargements (approx. 125% life-size) using a hand-held digital caliper. The repeatability of these measurements was about ±0.1 mm, suggesting error estimates of 2–4% for typical turbulent and laminar fringes, respectively, in the worst case when only a single fringe was measured. This is not insignificant, but could be reduced with greater enlargement of the photographs, digital imaging (either digitized from film or high-resolution digital), narrower filtration of the light source for sharper fringes, etc.

Once a calibrated viscosity of the DC-200 Fluid is substituted for the nominal value, the remaining uncertainty due to oil characteristics is small, on the order of 1%. If the other error sources were reduced as discussed, it might be worthwhile to verify all the physical properties of the oil. The geometrical correction factor [5] involving the cosines of the angles of incidence and refraction (in oil) is negligibly small: a 10-degree incidence angle, for instance, would lead to a skin friction error of less than 1%.

3.6 Discussion

In this demonstration experiment, we have obtained both qualitative and quantitative information about the boundary layer state and skin friction for the Ref H configuration. The regular zigzags in C_f in the wake of the trip disks were not expected, and they made it difficult to determine transition location as precisely as was hoped. Nevertheless, it was quite apparent that the disks were having an effect, and that the boundary layer was tripping well upstream of the free transition location. This had not been completely clear prior to the test.

The quantitative results are preliminary in nature. It became clear during the trial that several aspects of the technique can be improved, and others emerged after comparison with CFD results. Measurement of the oil temperature is important, especially under supersonic conditions, and the effects of wind tunnel start-up and shutdown transients require study, although this is apt to be expensive. Oil viscosity must be determined for each application, as was done here, but the other oil properties also deserve attention. More-precise illumination is easily achieved with appropriate filtration. Aside from methodological issues, the error can be reduced to about ±5% as follows: (1) measure surface temperature to ±0.5 K (1% error in C_f), (2) reduce transient effects to ±4% (or better) by additional runs up to three times as long, (3) use a better filter (±1%), (4) improve fringe measurement accuracy to ±1%, and (5) verify all the oil properties. At this level of accuracy, the oil-film method would be roughly competitive with other skin friction techniques and perhaps be especially valuable because its biases differ from those of other direct methods.

Oil-film interferometry helped to confirm that the trip disks were promoting transition. The quantitative skin friction measurements were sufficiently accurate to judge boundary layer state but not to permit critical comparison with CFD results. Precise transition location measurements proved elusive, but the sublimation technique to be described in the next section was used successfully to track movement of the transition front as the height of the trip devices was varied.

4 TRANSITION LOCATION USING A SUBLIMING CHEMICAL SOLID

4.1 Background

Flow visualization with a subliming solid has been used to indicate boundary layer transition since the 1940s. The method is discussed in some detail by Main-Smith [20], who credits unpublished work in 1945 by Pringle and Main-Smith. Another lengthy treatment is presented by Owen and Ormerod [21], who acknowledge a still-classified report by Gray published in 1944. All of this work was concerned with subsonic flow; see also the text by Rae and Pope [22]. In a quantitative application of the sublimation technique to supersonic flow, Vaucheret [23] describes the use of measured transition locations to correct drag data for the effects of laminar run and trip drag.

Following Vaucheret, our transition measurements together with estimates of the drag decrement for a mixed laminar-turbulent boundary layer relative to a fully turbulent one were used to compensate for the effect of laminar flow on the model (assuming consistent flow topology). With all the data now on an equal footing, a second correction for the drag due to the trip devices could be studied. Unlike Vaucheret, we found that on a portion of the wing, turbulence began downstream of the trip devices for even the largest sizes tried, well into the size range where trip drag is seen. This delay was probably due to the highly favorable pressure distribution on the inboard wing, where the leading edge is blunt. Further background on laminar run and trip drag corrections may be found in the recent paper by Goodsell, Kennelly, and Lawrence [24]. The discussion to follow will emphasize flow visualization aspects of that work.

4.2 Sublimation Experiments

Cruise performance testing of the TCA configuration was initially performed during January–February 1997. When the sublimation images used to confirm the effectiveness of the trip disks were closely examined, it was realized that transition was not occurring as close to the line of

disks as first thought. A second test entry in May–June 1999 provided the opportunity to extend the range of trip heights as well as to repeat some of the cases from the previous test. Tunnel conditions for the flow visualization results to be presented were $Ma = 2.40$ and $Re = 4.0$ million/ft (13.13 million/m). Lift, drag, and sublimation data were obtained for the bare-metal model (free transition) and for trip heights ranging from 0.002 to 0.017 inch (0.05 to 0.43 mm).

As in the oil-film experiment, the trip devices consisted of molded disks of automotive body filler ('glazing compound'), located 0.6 inch (15.2 mm) from the wing leading edge in the streamwise direction. They were formed using pre-punched tape with 0.050 inch (1.27 mm) diameter holes spaced 0.100 inch (2.54 mm) center-to-center. This disk spacing, that of the tape itself, was used on unswept edges, while every other disk was removed on the wing leading edges. Subsequent experience suggests that a larger spacing, perhaps 0.300 inch (7.62 mm), would be preferable on the highly swept (approx. 70 deg) inboard portion of the wing. The thickness of the tape served to produce disks of roughly consistent height; this was fine-tuned by hand shaving and measuring each disk individually, a time-consuming process. Trip disk heights were sampled to monitor their size and consistency. Two statistical criteria were applied: it was required that the average height be within 0.0005 inch (0.013 mm) of the nominal value specified and the standard deviation of the heights had to be less than 0.00025 inch (0.006 mm).

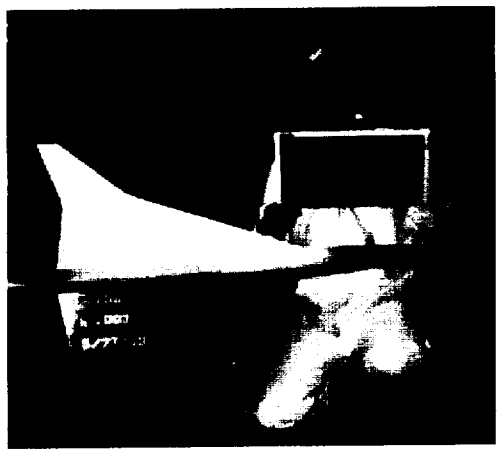

Figure 6. Technician in protective suit with the TCA model prepared for a sublimation run.

The transition location for each trip height was determined at the cruise angle of attack, $\alpha = 3.5°$, from sublimation photographs of the upper and lower wing surfaces. The sublimation material was a saturated solution of fluorene ($C_6H_4CH_2C_6H_4$) in Genesolv, a proprietary Freon solvent. An airless spray gun was used to apply the material directly to the (unpainted) stainless steel model. With practice, it is possible to apply a thick but fairly smooth coating by repeated light passes with the gun. One liter of solution was used for a typical upper and lower surface application. Consistency is difficult to achieve: some spray jobs exhibited a small degree of 'orange peel' surface texture, and the sublimation time varied from 20–60 minutes, depending upon run conditions and upon how thickly the material was sprayed on the model. Both the fluorene and the solvent are moderately toxic, and the aerosol that accumulates in the wind tunnel test section should not be inhaled. The technicians who applied the sublimation coatings wore a protective suit and respirator mask, and the test section was ventilated to clear the mist. A typical fluorene application is illustrated in Fig. 6, which also shows the protective gear required.

An unresolved issue is the effect of the thickness of the sublimation material on the action of the trip dots. In the second test entry, very small dot heights were used, approximately 0.002 inch (0.05 mm) tall; this is not much greater than the initial thickness of the fluorene coating. It would be preferable to limit application of the sublimation material to the region of interest behind the line of trip dots, but this must be done unobtrusively. An abrupt edge, as might be obtained by simply masking off the leading edge of the wing, could interfere with the transition process as much as partially submerging the dots in sublimation material.

Two 70-mm cameras, motorized and equipped with high-capacity film backs (Victor Hasselblad AB, Göteborg, Sweden), recorded the upper and lower wing surfaces on ISO 400/27° black-and-white negative film. Once tunnel conditions had stabilized, pictures were taken at one-minute intervals until most of the fluorene had sublimed. Since the flow conditions and spray thickness are generally not uniform over the model, it is necessary to monitor all regions of interest to avoid premature termination of the run. Our experience suggests that the common technique of relying upon a single photograph (often taken after a run) will be misleading unless the sublimation rate is the same everywhere on the model and the single photograph is made at just the right time.

Both steady and flash illumination were tried. The former is easier to set up to minimize glare, but flash is (usually) *brighter*, permitting smaller apertures and thus greater depth of field, and *briefer*, reducing unsharpness due to model motion. The effective exposure time is typically 1/500 sec or less (shorter than the camera's flash synchronization shutter speed). Depth of field was not properly appreciated at first since the wing provided a nearly planar subject. With a very wide-angle lens (f = 40 mm) at close distance (0.9 m), it was difficult to focus accurately despite use of a ground glass camera back and magnifying loupe. Experimentation revealed an inherent imprecision of about ±5 cm, which may have affected the quality of the images in some cases. In retrospect, we would have benefited from an aperture even smaller than the *f*/11 used in the examples below.

Following each run, a subset of the negatives (typically six) was chosen for analysis. These were digitized and stored in PRO PhotoCD format (Eastman Kodak, Rochester, NY, USA). It proved convenient to overlay the digitized images, lay out the transition front, and perform the measurements using Illustrator (Adobe Systems, San Jose, CA, USA) on a personal computer. Relative distances from wing leading edge and fuselage centerline to transition location were converted to absolute quantities by scaling from the known geometry of the wing (fiducial marks would have been useful). The laminar run correction, $\Delta C_{D_{lam}}$, was estimated from compressible, flat-plate skin friction formulae applied to ten or more strips on each wing surface. The required quantity is the difference between the fully turbulent drag and that of a mixed laminar-turbulent flow, Eq. (2), where the laminar and turbulent portions of the mixed boundary layer are patched together by matching momentum thicknesses at the measured transition location.

$$\Delta C_{D_{lam}} = \sum_i \left\{ C_{D_i}{}^{turb}(flat\ \ plate) - C_{D_i}{}^{lam-turb}(flat\ \ plate) \right\} \qquad (2)$$

4.3 Visualization results

Transition was found to be delayed over a wide range of trip disk heights, especially on the upper, inboard surface of the wing where the leading edge was blunt. While mapping the transition front for the free transition case was fairly easy (see Fig. 7), it was much less straightforward to measure the gradual movement of transition as the trip height was varied.

Figure 7. Sublimation image of TCA model upper wing surface (one of a series), free transition.

In several locations on the wing, a disk was isolated by removing two or three of its neighbors on each side. This makes the wake of an individual disk more visible so that the beginning of the characteristic 10–15 degree 'wedge' indicating transition is easily seen. We found that it is necessary to wait for the emergence of this pattern. Two enlarged, inboard-wing sublimation images will illustrate why this is important. The strongly scrubbed (dark) regions sometimes found behind the disks early in a run (see Fig. 8) have been incorrectly attributed to prompt transition by some observers. However, in Fig. 9, taken from later in the same k = 0.012 inch (0.30 mm) run, it is clear that transition is actually delayed. The beginning of the wedge behind the isolated disk, and, correspondingly, the locations where the 'fingers' of sublimation material between the other disks begin to narrow, were used to determine $\Delta C_{D_{lam}}$. The trip disks are taller than the impinging laminar boundary layer and satisfy Braslow's criteria for prompt transition [25], but are seen to be less effective than would have been anticipated for flat-plate flow. This delayed-transition behavior on the upper, inboard wing surface greatly complicated the analysis of trip drag. For further discussion of the interpretation of the sublimation images and maps showing the progression of transition location as a function of trip disk height, see Goodsell et al. [24].

Figure 8. Scrubbed areas visible behind disks early in run, k = 0.012 inch. Airflow is from right to left.

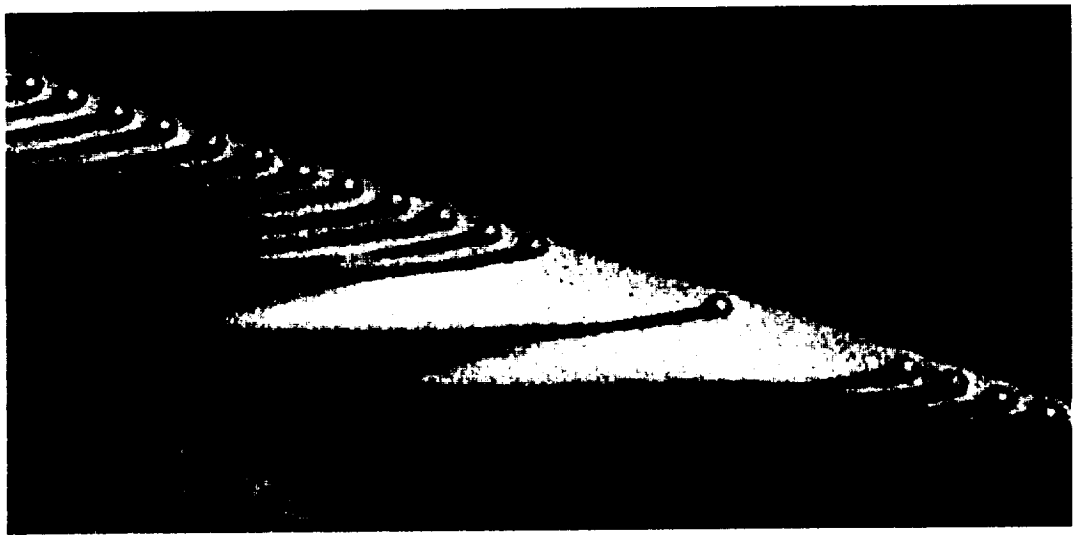

Figure 9. Transition wedge downstream of an isolated disk, k = 0.012 inch.

4.4 Errors

The laminar run corrections derived from the sublimation images have some uncertainty associated with them. The portion of this uncertainty due to the way that the transition front is mapped out may be estimated. Several of the runs were re-analyzed using different, plausible criteria for selecting transition location. In addition, several of the trip heights were repeated in a second test entry with different camera position, lighting, etc. Based on these repeated measurements, we feel that an uncertainty estimate of ±0.2 drag counts is reasonable for the free transition case and for trip heights of 0.006 inch and greater. This uncertainty is small compared to the laminar run correction for all but the largest trip sizes studied. (One 'count' is a drag coefficient increment of 0.0001.) In geometrical terms, 0.2 counts is equivalent to a uniform shift in model-scale transition location of 0.1 inch (2.5 mm) on both upper and lower wing surfaces.

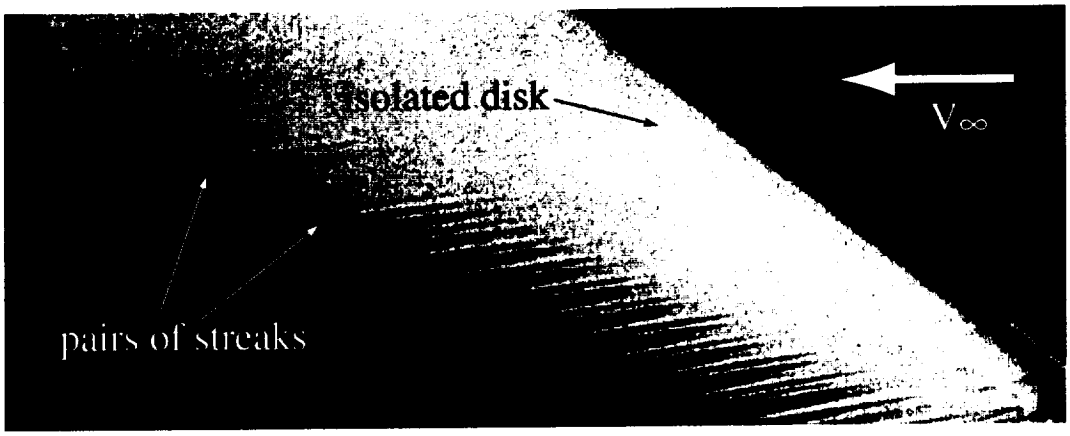

Figure 10. Sublimation image of outboard wing showing distinct pairs of lines, k = 0.002 inch.

For the two smallest trip heights, k = 0.002 and 0.004 inch, the uncertainty associated with locating transition is larger than for the other trip heights due to greater difficulty interpreting the sublimation images. The transition front for these cases did not stabilize as it did for the other trip configurations, and this made it difficult to identify the transition location with confidence. Additional doubt was caused by the appearance on the outboard, upper surface of features unlike either the feathery pattern seen in Fig. 7 or the wedges in Fig. 9. The new pattern, shown in Fig. 10, consists of pairs of sharply defined streaks of sublimation material extending well downstream behind each disk. A row of trip disks is present, though indistinct in the photograph, except where two disks have been removed on each side of the isolated disk. We chose to locate transition near the ends of these streaks because their length is consistent with the overall light-to-dark gray pattern evident in earlier images from the run, and because they are relatively stable (more so than the light-to-dark gray pattern). The flow mechanism that creates these streaks is unclear. Because the interpretation of the k = 0.002 and 0.004 inch sublimation images was somewhat tentative, the error estimate for $\Delta C_{D_{lam}}$ was increased to ±0.4 drag counts. A more detailed discussion of these and other sources of error may be found in Goodsell et al.

4.5 Laminar run and trip drag corrections

For completeness, the final laminar run and trip drag corrections deduced from the flow visualization images are presented in Fig. 11. The laminar run correction, $\Delta C_{D_{lam}}$, decreases smoothly with trip height, as suggested by the dashed line in the figure. For each trip height, this quantity is added to the drag measured in the wind tunnel, $C_{D_{WT}}$, to give the drag corresponding to fully turbulent flow on the wing:

$$C_{D_{turb}} = C_{D_{WT}} + \Delta C_{D_{lam}} \tag{3}$$

The drag data corrected for laminar run were then plotted against trip height (not shown here). We observed that $C_{D_{turb}}$ was *insensitive* to trip height for $k = 0$ through 0.008 inch (0.20 mm), forming a 'drag plateau.' Above the plateau, i.e., for $k \geq 0.008$, $C_{D_{turb}}$ increases with trip height. These data are well represented by a linear fit denoted $C_{D_{fit}}(k)$. Now the trip drag can be evaluated, using the relationship between k and the inferred drag of the model with fully turbulent flow on the wing.

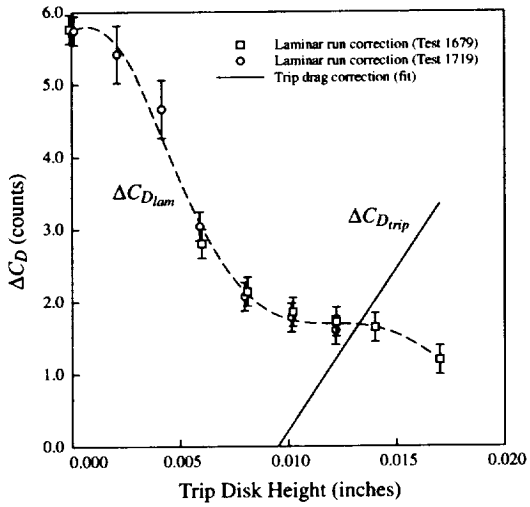

Figure 11. Laminar run and trip drag corrections.

The second correction, $\Delta C_{D_{trip}}$, accounts for the drag of the trip devices themselves. Below $k = 0.008$ inch (in the drag plateau), the trip drag is zero because we observed that $C_{D_{turb}}$ does not vary significantly with trip height. For larger trips, the correction is defined as the difference between the linear fit to $C_{D_{turb}}$ and the average plateau drag level $C_{D_{plateau}}$. This quantity, shown in Fig. 11 as a solid line, is positive and linear in k by construction; it must be subtracted from the laminar-run-corrected drag to obtain the final, fully corrected result, $C_{D_{corrected}}$

$$\begin{aligned} \Delta C_{D_{trip}} &= 0, && k \leq 0.008 \\ &= C_{D_{fit}}(k) - C_{D_{plateau}}, && k > 0.008 \end{aligned} \tag{4}$$

$$C_{D_{corrected}} = C_{D_{turb}} - \Delta C_{D_{trip}} \tag{5}$$

In these tests, the laminar run correction varied from one to six counts, while trip drag values range from zero to about three counts. It is noteworthy that although the laminar run investigation was originally motivated by a desire to quantify the trip drag, the two effects turn out to be of roughly equal importance for typical trip heights of $k = 0.010$ to 0.015 inch (0.25 to 0.38 mm).

4.6 Discussion

Quantitative use of the sublimation technique to map transition location as a function of trip height has clarified performance test results for a supersonic transport. It was essential to correct drag for laminar run. In contrast to some previous results, we found that the laminar boundary layer could extend past the trip disks, even for large trip heights. Only after this has been accounted for can the data be analyzed for trip drag. In both Vaucheret's results and the present work, plots of supersonic trip drag vs. trip height revealed a plateau region in which there is apparently no drag penalty associated with small trip elements. This observation is congruent with the *subsonic* results reported by Braslow, though not his supersonic observations. The absence of drag due to the trip devices remains somewhat surprising in either speed regime.

The laminar run and trip drag corrections required careful trip disk application and systematic measurement of transition location using multiple images from each run. This is time consuming, but the insight gained has suggested some hybrid approaches to tripping (or *not* tripping) the wing boundary layer that may facilitate future supersonic testing; see Goodsell et al. [24].

Finally, the distinctive flow pattern suggested by the sublimation images for the smallest trip heights presents an interesting puzzle. Since the twin streaks extend well downstream of the row of disks, perhaps the associated skin friction distribution should be studied with oil-film interferometry!

5 CONCLUDING REMARKS

This work has been motivated by the need to fully characterize the airflow over a wind tunnel model, in particular the state of the boundary layer. If a turbulent boundary layer is desired, artificial means are usually required to promote transition and thus the effect on drag of the boundary layer trip devices must be quantified. Two flow visualization techniques, oil-film interferometry and sublimation, provided complementary views of the boundary layer state on two supersonic transport models. Sublimation proved to be more suitable for visualizing transition location. In different ways, the two techniques revealed a highly disturbed region downstream of each trip disk. These disturbances are not, themselves, indicative of boundary layer transition; clarification of this point was a useful early conclusion of this work.

Quantitative results were also obtained. Skin friction measurements were made using oil-film interferometry to an estimated accuracy of roughly ±15%. More accurate results for local skin friction in compressible flow will require measurement of model surface temperature. A systematic investigation of the transient effects of starting and stopping the wind tunnel is also needed. The second technique presented, use of sublimation to measure and account for boundary layer transition location, yielded more concrete results. Once the problem of delayed transition on the upper, inboard surface of the wing was recognized, the sublimation images together with flat-plate skin friction estimates were used to quantify the effect of laminar flow on drag. Only after this laminar run correction had been performed was it possible to evaluate trip drag.

We have benefited from numerical methods, for example the CFD results for skin friction and wall temperature shown with the oil-film results. Such skin friction measurements may eventually contribute to better selection of appropriate computational grids or turbulence models. Meanwhile, planning and analysis of experiments can be improved by access to the level of detail provided by CFD. In the analysis of the sublimation data, described more fully in another paper, computed results for boundary layer quantities such as velocity, Mach number, and height-based Reynolds number were found to be useful improvements over flat-plate estimates.

ACKNOWLEDGEMENTS

The authors acknowledge the assistance of Jeffrey Flamm (NASA Langley) in the conduct of the oil-film test. That work also benefited from discussions with Russell Westphal (Washington State University), Aaron Drake (Raytheon Aircraft), and David Driver (NASA Ames). We thank Scott Lawrence (NASA Ames) for the computational results. Mina Cappuccio (NASA Ames) and Kevin Mejia (Boeing) participated in the sublimation tests. David Tuttle (NASA Langley) was Test Engineer, and Paul Bagby (NASA Langley) was responsible for the sublimation photography.

REFERENCES

[1] Whitehead, Allen H., Jr.: Status of NASA High-Speed Research Program. In *Fluid Dynamics Research on Supersonic Aircraft*. NATO RTO-EN-4. Rhode-Saint-Genèse, Belgium. 25–29 May 1998.

[2] Jackson, Charlie M., Jr., William A. Corlett, and William J. Monta: Description and calibration of the Langley Unitary Plan Wind Tunnel. NASA TP 1905. November 1981.

[3] Tanner, L.H., and L.G. Blows: A study of the motion of oil films on surfaces in air flow, with application to the measurement of skin friction. *J. Phys. E: Sci. Inst.* 9 (3): 194-202, 1976.

[4] Tanner, L.H., and V.G. Kulkarni: The viscosity balance method of skin friction measurement: further developments including applications to three-dimensional flow. *J. Phys. E: Sci. Inst.* 9 (12): 1114-21, 1976.

[5] Monson, Daryl J., George G. Mateer, and Florian R. Menter: Boundary-layer transition and global skin friction measurement with an oil-fringe imaging technique. SAE Paper 932550. Presented at Aerotech '93, Costa Mesa, CA, USA. 27–30 September 1993.

[6] Mateer, George G., Daryl J. Monson, and Florian R. Menter: Skin-friction measurements and calculations on a lifting airfoil. *AIAA Journal* 34 (2): 231–6, 1996.

[7] Kennelly, Robert A., Jr., Russell V. Westphal, George G. Mateer, and Julie Seelen: Surface oil film interferometry on a swept wing model in supersonic flow. In *Flow visualization VII: Proc. of the Seventh Int. Symposium on Flow Visualization,* ed. J.P. Crowder, 302–7. New York: Begell House, 1995.

[8] Driver, David M.: Application of oil-film interferometry skin-friction to large wind tunnels. In *Advanced Aerodynamic Measurement Technology.* AGARD CP-601. Presented at the 81st Fluid Dynamics Panel Symposium, Seattle, WA, USA. 22–25 September 1997.

[9] Drake, Aaron: Effects of cylindrical surface protrusions on boundary layer transition. Ph.D. dissertation, Washington State University, 1998. Available from University Microfilms, Ann Arbor, MI, USA.

[10] Drake, Aaron, Russell V. Westphal, Robert A. Kennelly Jr., and David M. Driver: Skin friction downstream of boundary layer trips. Paper 258, 8th Int. Symposium on Flow Visualization, Sorrento, IT. 1–4 September 1998.

[11] Westphal, Russell V., Aaron Drake, Robert A. Kennelly Jr., and David M. Driver. 1998. Interferometric skin friction footprint for tripped boundary layers. *Physics of Fluids* 9 (10): S5. Winning poster in the APS/DFD Flow Visualization Gallery Competition, San Francisco, CA, 23–25 November 1997.

[12] Zilliac, Gregory G.: Further developments of the fringe-imaging skin friction technique. NASA TM 110425. December 1996.

[13] Zilliac, Gregory: Skin friction distribution on a wingtip. AIAA Paper 98-0584. Presented at the 36th Aerospace Sciences Meeting and Exhibit, Reno, NV, USA. 12–15 January 1998.

[14] Drake, Aaron, and Robert A. Kennelly Jr.: Oil film interferometry for skin friction measurement on an aircraft in flight. Paper 292, 8th Int. Symposium on Flow Visualization, Sorrento, IT. 1–4 September 1998.

[15] Drake, Aaron, and Robert A. Kennelly Jr.: In-flight skin friction measurements using oil film interferometry. *J. Aircraft* 36 (4): 723–5, 1999.

[16] Gregory, N., and W.S. Walker: The effect on transition of isolated surface excrescences in the boundary layer. Aero. Res. Council R. & M. No. 2779. October 1951.

[17] van Driest, E.R., and W.D. McCauley: The effect of controlled three-dimensional roughness on boundary-layer transition at supersonic speeds. *J. Aero/Space Sciences* 27 (4): 261–71, 303, 1960.

[18] Westphal, R.V., R.A. Kennelly Jr., and A. Drake: Skin friction footprint of the vortex/boundary layer interaction. Paper 320, 9th Int. Symposium on Flow Visualization, Edinburgh, Scotland. 22–25 August 2000.

[19] White, Frank M.: *Viscous Fluid Flow.* 2nd ed. New York: McGraw-Hill, 1991.

[20] Main-Smith, J.D. 1950. Chemical solids as diffusible coating films for visual indications of boundary-layer transition in air and water. Aero. Res. Council R. & M. No. 2755.

[21] Owen, P.R., and A.O. Ormerod. 1951. Evaporation from the surface of a body in an airstream (with particular reference to the chemical method of indicating boundary-layer transition). Aero. Res. Council R. & M. No. 2875.

[22] Rae, William H., Jr., and Alan Pope: *Low-Speed Wind Tunnel Testing.* 2nd ed. New York: John Wiley & Sons, 1984.

[23] Vaucheret, X. Artificial initiation of the supersonic transition. NASA TT-F-11558. 1968. First published as Declenchement artificiel de la transition en supersonique. *La Recherche Aerospatiale,* no. 120 (September–October 1967): 25–32.

[24] Goodsell, Aga M., Robert A. Kennelly Jr., and Scott L. Lawrence: Accounting for laminar run and trip drag in supersonic cruise performance testing. AIAA Paper 2000–0265. Presented at the 38th Aerospace Sciences Meeting and Exhibit, Reno, NV, USA. 10–13 January 2000.

[25] Braslow, Albert L., Raymond M. Hicks, and Roy V. Harris, Jr.: Use of grit-type boundary-layer-transition trips on wind-tunnel models. NASA TN D-3579. September 1966.